Archives of Toxicology (2022) 96:2049–2065
https://doi.org/10.1007/s00204-022-03297-z

GENOTOXICITY AND CARCINOGENICITY

Circular RNA circNIPBL promotes NNK-induced DNA damage in bronchial epithelial cells via the base excision repair pathway

Yufei Liu[1,2] · Qiuhan Hua[1,2] · Meizhen Li[2] · Xueqi Li[2] · Wei Chen[2] · Huixian Zeng[2] · Qinqin Diao[2] · Changhong Shi[2] · Yihui Ling[2] · Yiguo Jiang[1,2]

Received: 25 October 2021 / Accepted: 31 March 2022 / Published online: 18 April 2022

Abstract

Environmental chemical exposure often causes DNA damage, which leads to cellular dysfunction and the development of diseases. 4-(Methylnitrosamino)-1-(3-pyridyl)-1-butanone (NNK), a tobacco-specific carcinogen that is known to cause DNA damage, while remains unknown about the underlying mechanism. In this study, simulated doses of NNK exposure in smokers, ranging from 50 to 300 μM, were used to detect the DNA damage effects of NNK in two human bronchial epithelial cells, 16HBE and BEAS-2B. The comet assay revealed increased DNA damage in response to NNK treatment, as measured by increased Olive tail moment (OTM). NNK treatment also led to elevated foci formation and protein expression of γ-H2AX, a DNA damage sensor. Dysregulation of proliferation, cell cycle arrest and apoptosis, was also observed in NNK-treated cells. Furthermore, the most effective dose of NNK (300 μM) was used in subsequent mechanistic studies. A circular RNA circNIPBL was identified to be significantly up-regulated in NNK-treated cells, circNIPBL knockdown successfully alleviated NNK-induced DNA damage and reversed the cellular dysregulation, while circNIPBL overexpression had the opposite effect. Mechanistically, we identified an interaction between circNIPBL and PARP1, a critical enzyme of the base excision repair (BER) pathway. CircNIPBL silencing successfully alleviated the NNK-induced inhibition of BER pathway proteins, including PARP1, XRCC1, PCNA and FEN1, while overexpression of circNIPBL had the opposite effect. In summary, our study shows for the first time that circNIPBL promotes NNK-induced DNA damage and cellular dysfunction through the BER pathway. In addition, our findings reveal the crucial role of epigenetic regulation in carcinogen-induced genetic lesions and further our understanding of environmental carcinogenesis.

Keywords NNK · Circular RNA · DNA damage · Base excision repair · PARP1

Introduction

Non-coding RNAs (ncRNAs), including microRNAs (miRNAs), long non-coding RNAs (lncRNAs) and circular RNAs (circRNAs), are important modulators of epigenetic regulation, which has an important role in mediating diverse biological processes and human diseases. In the past decade, several ncRNAs, including miRNAs and lncRNAs, have been identified in health hazards resulting from environmental chemicals by our research group and others (Li et al. 2013; Luo et al. 2021; Pan et al. 2019).

CircRNAs are expressed in cell type- and tissue-specific patterns, and are highly conserved and stable, in part due to their single-stranded covalently closed-loop structures, which lack 5′–3′ polarity and poly(A) tails (Li et al. 2018; Wang et al. 2020b). Our previous studies have described an important role of circRNAs during environmental compound-induced biological malfunction and carcinogenesis. For example, circ_CARM1 was shown to competitively bind to miR-1288-3p, thereby regulating the migration of BPDE-transformed human bronchial epithelial cells, while circ_0035266 was found to promote the inflammatory response caused by tobacco exposure via the miR-181d-5p/

Yufei Liu and Qiuhan Hua have contributed equally to this work.

✉ Yiguo Jiang
jiangyiguo@vip.163.com; jiangyiguo@gzhmu.edu.cn

[1] State Key Laboratory of Respiratory Disease, The First Affiliated Hospital of Guangzhou Medical University, Guangzhou 510120, China

[2] Institute for Chemical Carcinogenesis, Guangzhou Medical University, Xinzao Town, Panyu District, Guangzhou 511436, China

DDX3X axis (Hua et al. 2021; Xiao et al. 2021). Although the role of circRNAs as miRNA sponges is well established, circRNAs have also been found to exert their biological function by interacting with different proteins. Previously, we have demonstrated that circRNA 406,961 regulates PM 2.5-induced inflammatory responses by interacting with ILF2 protein (Jia et al. 2020). Although circRNAs have been reported to play an important role in a variety of biological dysfunction, few studies have focused on their role in the regulation of genetic lesions.

DNA damage, the most representative genetic lesion, is one of the earliest events during carcinogenesis, and may alter the genetic sequences that affect cellular processes and the initiation of malignant phenotypes (Basu 2018; Roos et al. 2016). Several studies have shown that circRNAs have inevitable functions in modulate DNA damage by acting as miRNA sponges or affecting RNA-binding protein (RBP) interaction patterns (Malakoti et al. 2021). For example, Han et al. found that circITCH could serve as a sponge for miR-330-5p in hiPSC-CMs to promote SIRT6 expression, a critical member of the sirtuin family involved in DNA repair and the maintenance of genomic stability (Han et al. 2020). In addition, the circRNAs, CDR1as and cCNTNAP3, were reported to modulate the expression of p53 protein, an important tumor suppressor, which has been implicated in the regulation of DNA repair, cell cycle arrest, and apoptosis (Levine and Oren 2009; Lou et al. 2020; Wang et al. 2020a). However, the established role of circRNAs in regulating DNA damage, especially damage caused by environmental chemicals, as well as the molecular mechanisms of circRNAs within this context remain largely absent.

The occurrence of DNA damage is associated with a myriad of endogenous and exogenous genotoxic insults. Chemical carcinogens, one kind of risk factors for cancer etiology, have been reported to induce various forms of DNA damage such as DNA-strand breakage, DNA-strand crosslinking, chromosomal rearrangements, and DNA-adduct formation (Barnes et al. 2018; Poirier 2004). A typical example is tobacco smoke, the most prevalent environmental risk factor for several types of cancer, due to a process driven by over 60 carcinogenic compounds that directly damage and mutate DNA. 4-(Methylnitrosamino)-1-(3-pyridyl)-1-butanone (NNK) is one of the most abundant and highly carcinogenic *N*-nitrosamines (Yoshida et al. 2020). Specifically, NNK is a genotoxic carcinogen that contributes to the formation of DNA adducts via the metabolism of cytochrome P450 enzymes, which in turn leads to genomic instability and the onset of programmed cell death, such as apoptosis (Balbo et al. 2014).

Cigarette smoke and NNK treatment have been shown to trigger DNA double-strand breaks (DSBs) in vitro via the phosphorylation of histone H2AX at serine 139 (γ-H2AX), a sensitive biomarker for DNA DSB detection (Ibuki et al. 2015; Zhao et al. 2009). In response to DSBs, ataxia telangiectasia mutated kinase (ATM) is recruited by γ-H2AX and, once phosphorylated, γ-H2AX initiates DNA damage repair and downstream protein activation, which in turn leads to senescence, cell cycle arrest, apoptosis or DNA repair (Amararathna et al. 2020; Saitoh and Oda 2021; Zhao et al. 2009). In addition, nucleotide excision repair (NER), mismatch repair (MMR) and base excision repair (BER) pathways have been shown to be involved in NNK- or cigarette smoke-induced DNA damage repair (Brown and Massey 2009; Doukas et al. 2020; La Maestra et al. 2011). However, the underlying mechanism behind NNK-induced DNA damage and involvement of circRNA remain unclear.

In the present study, we confirmed that NNK exposure induces DNA damage in two human bronchial epithelial cell lines 16HBE and BEAS-2B, and identified the circRNA, circNIPBL (circBase ID: has_circ_0001472), which was significantly up-regulated in response to NNK treatment. Next, we demonstrated that circNIPBL could promote NNK-induced DNA damage by modulating the BER pathway through interactions between circNIPBL and poly (ADP-ribose) polymerase (PARP1). Taken together, our data identify a novel mechanism underlying circNIPBL in NNK-induced DNA damage, and provide novel insights into the epigenetic regulation of genetic lesions.

Material and methods

Cell culture and NNK treatment

16HBE cells were obtained from the Guangzhou Institute of Respiratory Diseases, and cultured in Modified Eagle's Medium (MEM) containing 10% fetal bovine serum, as described previously (Hua et al. 2019). BEAS-2B cells were cultured in serum-free Bronchial Epithelial Cell Growth Medium (Lonza, Switzerland), and HEK 293-T cells were grown in high glucose Dulbecco's MEM (DMEM). All cells were cultured in a humidified atmosphere consisting of 5% CO_2 at 37 °C.

NNK (99.9% purified) was purchased from Toronto Research Chemicals (TRC, Toronto, Canada), dissolved in phosphate buffered saline (PBS) containing toxicity negligible 0.1% DMSO to a final concentration of 100 mM, and stored at − 20 °C. To determine realistic simulated doses of NNK for this study, we considered the levels of NNK in cigarettes and average cigarette consumption of habitual smokers. The amount of NNK in tobacco ranges from 12 to 110 μg/cigarette (0.058–0.53 μmol/cigarette), while the habitual smoker consumes about 20 cigarettes per day (Konstantinou et al. 2018). The lung volume of adults (ranging from 2000 to 5000 mL) and low cytotoxicity were also considered to determine suitable experimental doses. The

most significant damage time point was considered to be two months, and the accumulated concentration of NNK in two months ranged from 13.92 to 318 μmol. Thus, we used NNK at doses of 50, 100, 200 and 300 μM for subsequent experiments.

Reverse transcription and quantitative real-time PCR (qRT-PCR)

Total RNA was extracted using TRIzol reagent (Invitrogen, Carlsbad, CA, USA) according to the manufacturer's instructions. Reverse transcription was carried out using the Reverse Transcription System (Promega, Madison, WI, USA). qPCR Master Mix (Promega) was used for qRT-PCR. GAPDH was used as the internal control. The thermal cycle conditions and data analysis method have been described previously (Hua et al. 2019). All primers were synthesized by Sangon Biotech (Shanghai, China), and the sequences are shown in Supplementary Table S1.

Western blot analysis

Total protein was extracted from both cell lines using Cell Lysis Buffer for Western and IP (Biotechnology, Shanghai, China), and quantified using the BCA Assay Kit (Thermo Scientific, USA). Protein was separated on Precast PAGE Gels (Beyotime Biotechnology), then transferred to 0.4 μm PVDF membranes. Membranes were incubated with primary antibodies for 2 h at room temperature or overnight at 4 °C, then incubated with specific IRDye® 800CW secondary antibodies. Protein bands were scanned and quantified using ODYSSEY CLx (LI-COR, Nebraska, USA). The antibodies used in these experiments are shown in Supplementary Table S2.

Immunofluorescence staining

Pretreated cells that had been cultured on round coverslips were fixed in 4% paraformaldehyde, washed with 0.5% PBST (PBS containing 0.5% Tween20) and permeabilized with 0.5% TritonX-100 (diluted in PBST). Samples were blocked in bovine serum albumin (1% BSA in PBST), then incubated with primary antibodies overnight at 4 °C. The following day, coverslips were washed with PBST and incubated with Alexa Fluor® 488 fluorescent secondary antibody for 40 min followed by nuclear staining with DAPI. Images were acquired using a Leica SP8 confocal microscope.

Comet assay

A single-cell suspension was mixed with 0.7% low melting-temperature agarose and seeded onto slides. Post-solidification, slides were dipped in ice-cold lysis solution (2.5 M NaCl, 100 mM Na_2EDTA, 10 mM Tris) and lysed for 2 h in the dark at 4 °C. Slides were next incubated in an electrophoresis buffer to unwind the DNA helix, followed by electrophoresis in constant voltage conditions (25 V, 300 mA) for 30 min. Slides were washed in Tris–HCl (pH 7.5) and stained using NA-Red (Beyotime). Images for each group were captured by fluorescence microscopy, and CASP software was used to quantify the Olive tail moment (OTM) value of individual cells.

CircRNA screening and characteristic analysis

miRNAs were obtained based on DNA damage response (DDR)-related researches, and the most promising miRNAs were selected for circRNA prediction. Four circRNAs (hsa_circ_0001714, hsa_circ_0000990, hsa_circ_0001320, and hsa_circ_0001472) with promising functions and suitable sizes were selected for further validation. Prediction of potential binding circRNAs was carried out using the StarBase database (http://starbase.sysu.edu.cn/) based on CLIP experimental data and potential binding sites between miRNAs and circRNAs. Specific primers were designed that spanned the back-splice junction sites and amplified by qRT-PCR. The PCR products were used for Sanger sequencing to determine the correct junction sequence. To measure circRNA stability, 2 ng total RNA was treated with RNase R (Epicentre, USA) for 10 min, and circRNA expression was detected by qRT-PCR. The subcellular localization of circRNAs was determined by qRT-PCR on the RNA nuclear and cytoplasmic fractions, and fluorescence in situ hybridization (FISH). Nuclear and cytoplasmic fractions of RNA were isolated using the PARIS™ Kit (Life Technologies, USA) according to the manufacturer's instructions. The spanning junction site circRNA probe modified with 6-FAM was produced by Sangon Biotechnology. 16HBE cells were cultured on coverslips, fixed with paraformaldehyde and incubated with circRNA specific probes overnight at 37 °C. Cells were counterstained with DAPI and visualized by confocal microscopy. Information about the circNIPBL specific probe is shown in Supplementary Table S5.

Cell transfection

Small interfering RNAs (siRNAs) and overexpression vectors targeting circRNA were synthesized by GenePharma (Shanghai, China). The circRNA upstream intron (300 bp), circRNA (1574 bp) and downstream intron (300 bp) were included to construct the circNIPBL overexpression vector. The restriction enzymes BamHI and EcoRI were used to insert the above sequence into the pcDNA 3.1^+ expression vector. Lipofectamine 2000 (Invitrogen) was used for all circRNA knockdown and overexpression transfections. Briefly, cells were seeded into 6-well plates. Lipofectamine

(3 µL) was mixed in 1 mL OPTI-MEM, while 3 µL siRNA (20 mM) or 2 µL overexpression vector (1 µg/µL) was added to 1 mL OPTI-MEM and left to stand at room temperature for 5 min. After mixing, the solution was left to stand for a further 20 min, then added to the 6-well plates (1 mL per well) for 6–8 h. The media was replaced with conventional media and cells were harvested 48 h later. Circ_S1 (circRNA small interfering RNA 1) and circ_S2 (circRNA small interfering RNA 2) represent two different siRNAs specific for circNIPBL, while circ_NC (circRNA small interfering negative control) is a genome-wide negative control siRNA. Circ_OE (circRNA overexpression) is the overexpression vector for circNIPBL, and circ_vector (circRNA empty vector) is the empty vector control for circRNA overexpression. Information about the specific circNIPBL siRNAs and plasmids are shown in Supplementary Tables S3 and S4.

CCK8 assay

Cell viability was assessed using a Cell Counting Kit-8 (CCK8, Dojindo, Japan). Briefly, 5000 cells/well were cultured in 100 µL medium in a 96-well plate. The CCK8 reagent (10 µL) was added to each well at the following time points: 12 h, 24 h, 48 h, and 72 h. After 2-h incubation, absorbance values were read at 450 nm using a microplate reader (BioTek, Winooski, VT, USA). Cell growth curves were plotted using the average absorbance of each group.

5-Ethynyl-2′-deoxyuridine (EdU) assay

Since EdU is a thymidine (T) analogue, which can easily replace thymidine during cell proliferation, EdU can be used as a sensitive marker of proliferative activity. Here, the Cell-Light EdU Kit (Ribobio, Guangzhou, China) was used to detect EdU activity. Briefly, diluted EdU (1:1000 in medium) was added to treated cells and incubated overnight. Dyeing and image capture were performed the following day according to the manufacturer's instructions. Cells with a red fluorescent signal represented proliferating cells.

Cell cycle assay

The cell cycle was assessed by flow cytometry as described previously (Hua et al. 2019), and have made some optimizations. Briefly, cells were trypsinized, single-cell suspensions were prepared, and fixed using 70% ethanol at 4 °C overnight. Samples were washed with PBS, then incubated with RNase A/propidium iodide (v/v, 1:9) for 1 h. Cell cycle flow cytometry was performed on a CytoFLEX flow cytometer (Beckman Coulter, USA), and the resulting data were analyzed and visualized using flowJo software (Tree Star Inc., USA).

Fig. 1 NNK exposure induces DNA damage in human bronchial epithelial cells. **A** Representative comet assay images of NNK-treated cells. **B** Box plots showing OTM values of 200 individual cells detected by comet assay. **C** Western blot showing up-regulation of γ-H2AX expression levels in NNK-treated 16HBE cells. **D** Statistical histograms of relative γ-H2AX expression levels. **E** Representative γ-H2AX immunofluorescence images of NNK-treated 16HBE cells. **F** Statistical analysis of γ-H2AX immunofluorescence. **G**, **H** γ-H2AX expression levels in NNK-treated 16HBE cells at the indicated time points (0 h, 2 h, 4 h, 8 h, 12 h, 24 h, and 48 h). **I** Immunofluorescence staining showing NNK-induced γ-H2AX foci formation at different time points. **J** Statistical analysis of γ-H2AX foci formation

RNA sequencing

After the total RNA has been quality-tested, mRNAs of 16HBE cells are enriched using magnetic beads ligated to Oligo (dT). The extracted mRNA was randomly broken into short fragments in fragmentation buffers, and a first-strand cDNA was synthesized with six random hexamers using the fragmented mRNA as a template. Next, buffers, dNTPs, RNaseH, and DNA Polymerase I were added for two-strand cDNA synthesis. AMPure XP beads were used to purify the double-stranded products. T4 DNA polymerase and Klenow DNA polymerase were used to repair the sticky ends of the DNA to blunt ends, and to add linkers to the 3′ ends. AMPureXP beads were used for segment selection, and finally PCR amplification was performed to obtain the final sequencing library. After passing the quality inspection of the library, Illumina Novaseq™ 6000 was used for sequencing, and the sequencing length was 2 × 150 bp (PE150) at both ends.

CircRNA pull-down assay

Specific probes spanning the junction sites of circRNAs were designed to pull-down proteins potentially interacting with circRNA. Probes labeled with desthiobiotin were synthesized (Sangon Biotech), and incubated with total RNA (about 10^7 cells) at 70 °C for 5 min. Then, magnetic beads were added, agitated for 30 min, and washed with protein-RNA capture buffer. Next, the supernatant was discarded and the beads were incubated with a protein reacted mixture (containing 100 µg total protein) for 2 h at room temperature. Finally, proteins were eluted from the beads using elution buffer for 20 min at 37 °C. Eluted proteins were removed and examined by downstream mass spectrometry (MS) and western blotting. All the reagents described above were obtained from the Pierce™ Magnetic RNA–Protein Pull-Down Kit (Pierce Biotechnology, Rockford, USA). MS analysis was performed by Oebiotech (Shanghai, China). The circNIPBL specific probe used for the RNA pull-down assay shared the same sequence as the probe used for the FISH assay but was labeled in a different way (Supplementary Materials Table S5).

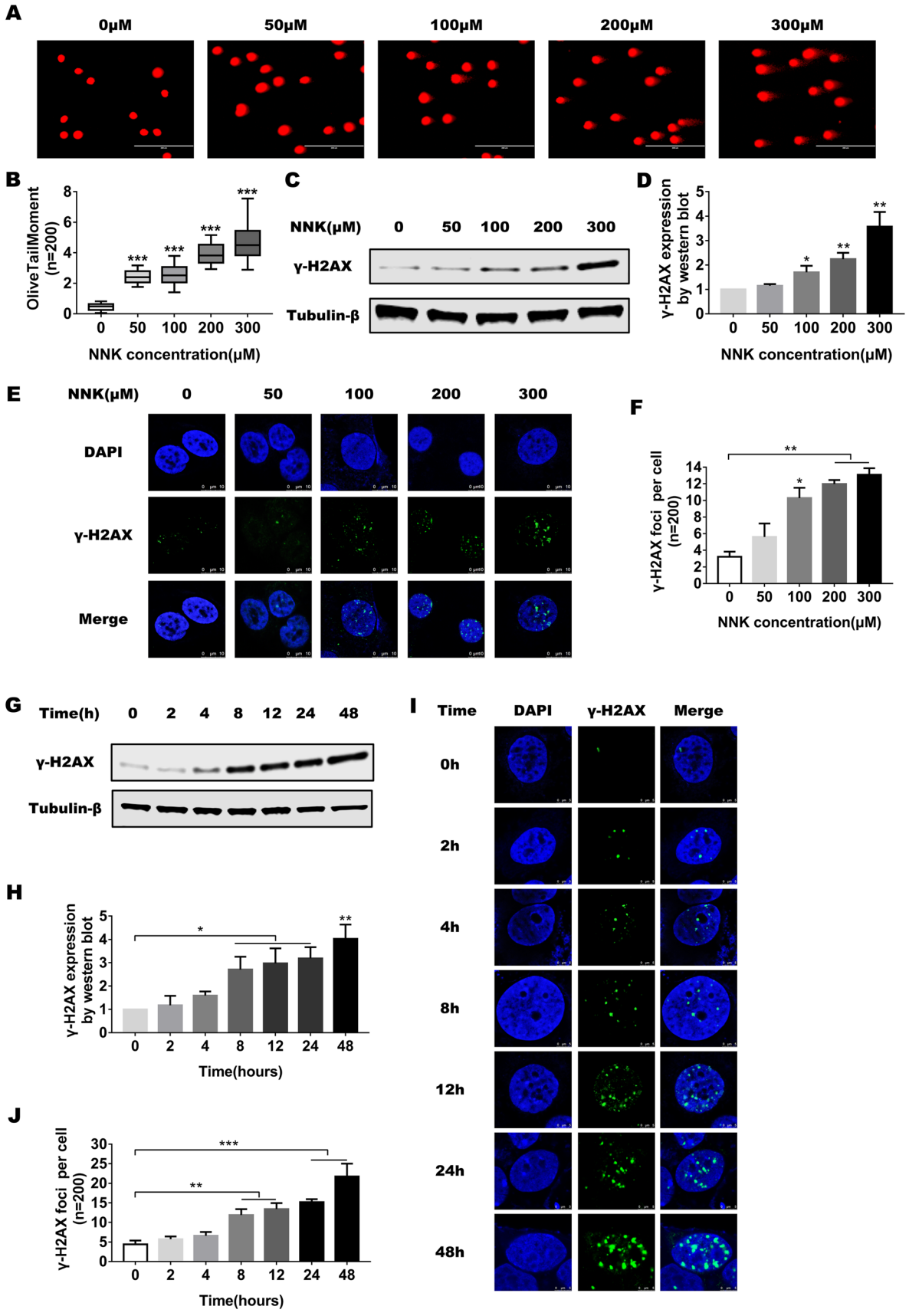
A
0μM
50μM
100μM
200μM
300μM
B
OliveTailMoment (n=200)
NNK concentration(μM)
C
NNK(μM) 0 50 100 200 300
γ-H2AX
Tubulin-β
D
γ-H2AX expression by western blot
NNK concentration(μM)
E
NNK(μM) 0 50 100 200 300
DAPI
γ-H2AX
Merge
F
γ-H2AX foci per cell (n=200)
NNK concentration(μM)
G
Time(h) 0 2 4 8 12 24 48
γ-H2AX
Tubulin-β
H
γ-H2AX expression by western blot
Time(hours)
I
Time DAPI γ-H2AX Merge
0h
2h
4h
8h
12h
24h
48h
J
γ-H2AX foci per cell (n=200)
Time(hours)

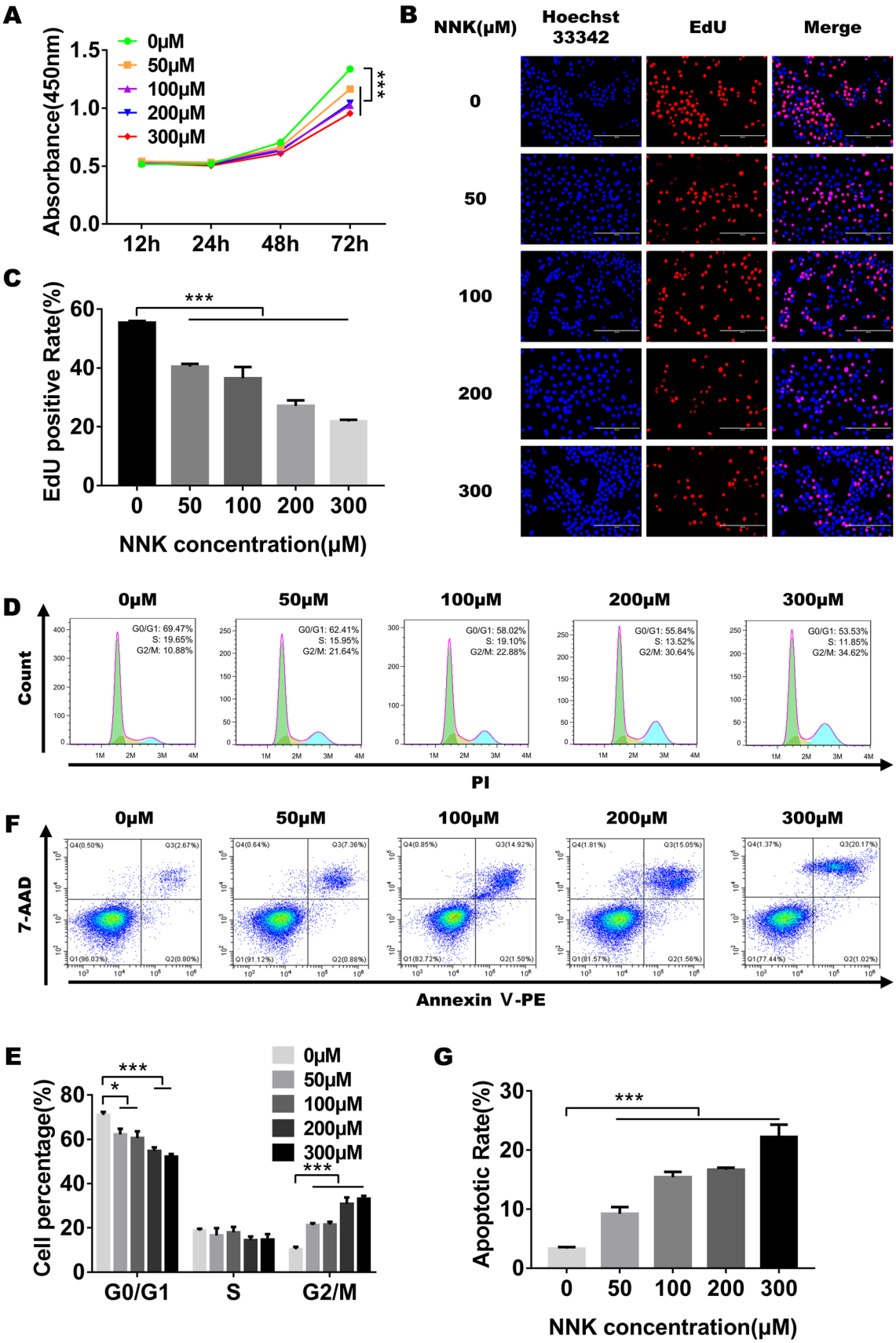
A
Absorbance(450nm)
0μM
50μM
100μM
200μM
300μM
***
12h
24h
48h
72h
B
NNK(μM)
Hoechst 33342
EdU
Merge
0
50
100
200
300
C
EdU positive Rate(%)
***
NNK concentration(μM)
D
0μM
50μM
100μM
200μM
300μM
Count
G0/G1: 69.47%
S: 19.65%
G2/M: 10.88%
G0/G1: 62.41%
S: 15.95%
G2/M: 21.64%
G0/G1: 58.02%
S: 19.10%
G2/M: 22.88%
G0/G1: 55.84%
S: 13.52%
G2/M: 30.64%
G0/G1: 53.53%
S: 11.85%
G2/M: 34.62%
PI
F
7-AAD
Annexin V-PE
E
Cell percentage(%)
G0/G1
S
G2/M
G
Apoptotic Rate(%)
NNK concentration(μM)

◂**Fig. 2** NNK exposure causes inhibition of cell proliferation, and induction of cell cycle arrest and apoptosis in 16HBE cells. Cells were treated with the indicated doses of NNK for 48 h. **A** CCK8 assay of 16HBE cells treated with the indicated doses of NNK. **B** EdU assays assessing the proliferative rate of NNK-treated cells. **C** Statistical analysis of EdU assay. **D** Cell cycle distribution of 16HBE cells detected by flow cytometry. **E** Statistical analysis of cell cycle distribution. **F** Flow cytometry detected NNK-induced apoptosis. **G** Apoptotic rate of NNK-treated 16HBE cells

Statistical analysis

Statistical analyses were carried out using SPSS 22.0 (IBM, Chicago, USA) and visualized by GraphPad Prism (San Diego, USA). Data are presented as average ± SD (standard deviation), from at least three independent experiments. $*P<0.05$, $**P<0.01$, $***P<0.001$. The statistical

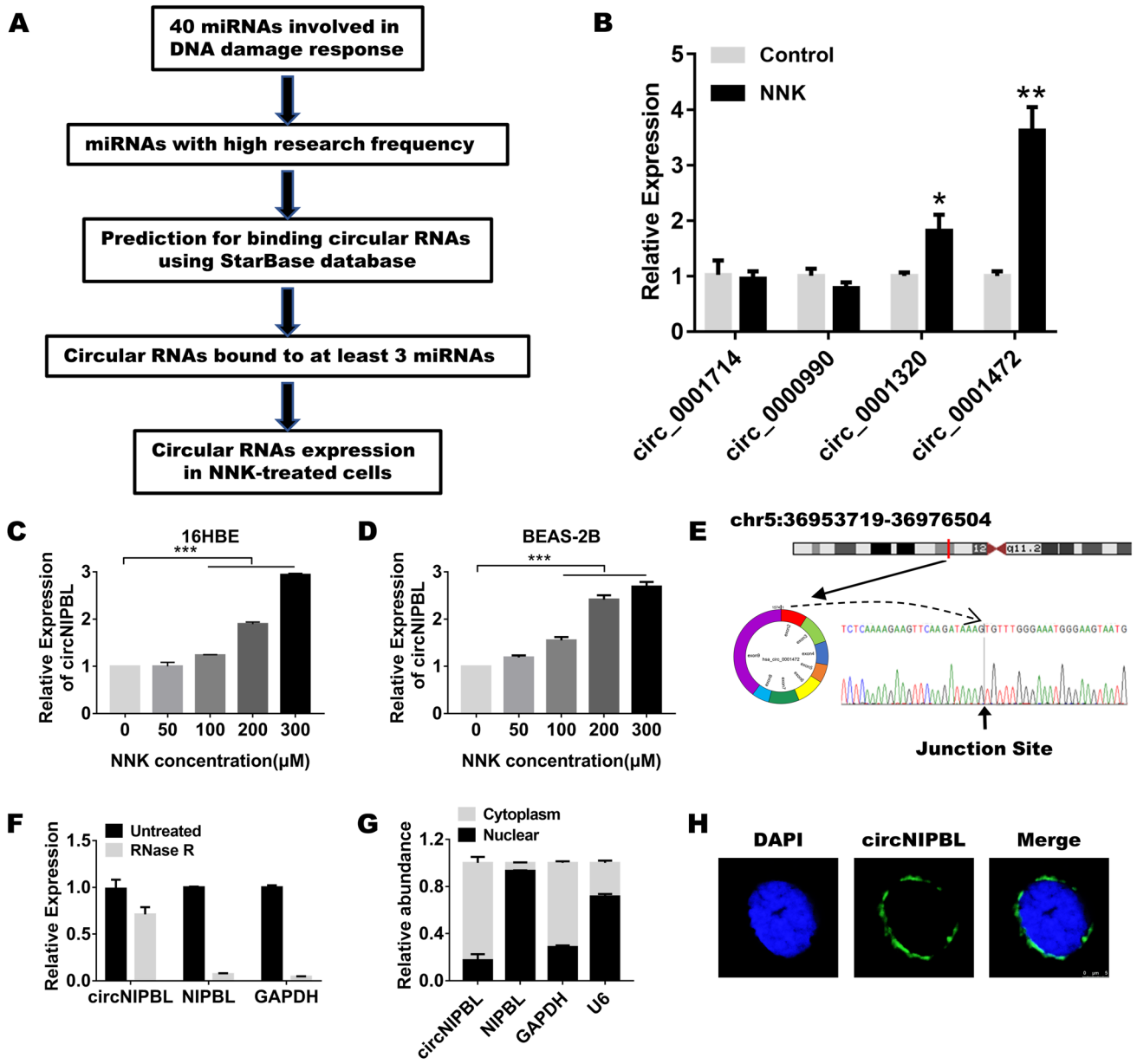

Fig. 3 Characterization of circNIPBL, which is up-regulated in NNK-treated human bronchial epithelial cells. **A** Flow diagram of circRNA screening. **B** qRT-PCR was used to verify expression of candidate circRNA. **C**, **D** Dose-dependent circNIPBL expression in bronchial epithelial cells was confirmed by qRT-PCR. **E** Genomic locus and exon composition of circNIPBL, wave curve indicates Sanger sequencing of the circNIPBL back-spliced junction site. **F** qRT-PCR analysis of RNase R resistance of circNIPBL. **G** The expression of circNIPBL, linear NIPBL, GAPDH and U6 in nuclear and cytoplasmic fractions was detected by qRT-PCR. **H** Subcellular localization of circNIPBL in 16HBE cells was detected by fluorescence in situ hybridization

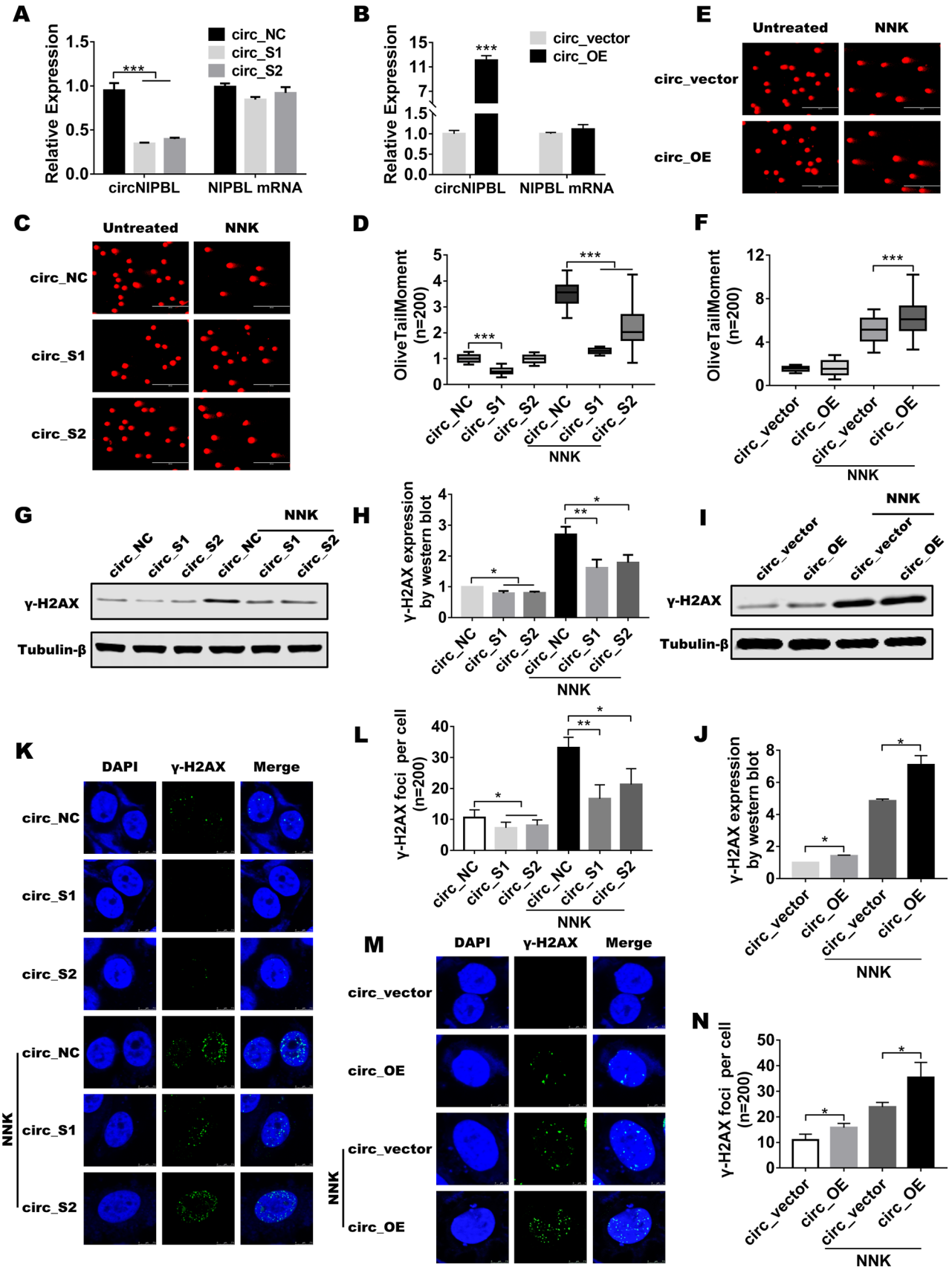
A
Relative Expression
circ_NC
circ_S1
circ_S2
***
circNIPBL
NIPBL mRNA
B
Relative Expression
circ_vector
circ_OE
***
circNIPBL
NIPBL mRNA
E
Untreated
NNK
circ_vector
circ_OE
C
Untreated
NNK
circ_NC
circ_S1
circ_S2
D
OliveTailMoment (n=200)
***
circ_NC
circ_S1
circ_S2
NNK
F
OliveTailMoment (n=200)
***
circ_vector
circ_OE
NNK
G
NNK
γ-H2AX
Tubulin-β
H
γ-H2AX expression by western blot
NNK
I
NNK
γ-H2AX
Tubulin-β
K
DAPI
γ-H2AX
Merge
NNK
L
γ-H2AX foci per cell (n=200)
NNK
J
γ-H2AX expression by western blot
NNK
M
DAPI
γ-H2AX
Merge
NNK
N
γ-H2AX foci per cell (n=200)
NNK

◂**Fig. 4** CircNIPBL promotes NNK-induced DNA damage by mediating γ-H2AX levels. **A**, **B** Knockdown and overexpression efficiency of circNIPBL was detected by qRT-PCR. **C**, **D** Representative comet assay images of circNIPBL-silenced 16HBE cells. Box plots show OTM values of 200 individual cells. **E**, **F** Overexpression of circNIPBL-aggravated DNA damage was verified by comet assay. **G**, **H** Western blot analysis was used to detect γ-H2AX expression levels in circNIPBL-silenced 16HBE cells. **I**, **J** γ-H2AX expression levels in circNIPBL-overexpressing 16HBE cells. **K**–**N** Immunofluorescence assays detected γ-H2AX foci formation in circNIPBL knockdown or overexpressed 16HBE cells

difference between two groups was analyzed by Student's *t* test. Multiple group comparisons were analyzed by One-way ANOVA, and Bonferroni's test was used for further two group comparisons. P values < 0.05 were considered to be statistically significant.

Results

NNK exposure induces DNA damage in human bronchial epithelial cells

16HBE cells were treated with different doses of NNK (0, 50, 100, 200, 300 μM) to determine its DNA damage induction capability. Comet assays suggested that NNK exposure significantly increased the average OTM value of 16HBE cells in a dose-dependent manner (Fig. 1A, B). Next, we examined the effects of NNK on γ-H2AX, a DNA damage sensor protein, by western blotting and immunofluorescence staining. We found that γ-H2AX protein levels increased gradually in response to NNK exposure in a dose-dependent manner. A 3.6-fold increase in γ-H2AX levels was observed after treatment with 300 μM NNK for 48 h compared to the control group (Fig. 1C, D). Moreover, we found that γ-H2AX foci formation in 16HBE cells was significantly increased by NNK treatment compared to controls. In particular, the highest increase in γ-H2AX foci formation was observed in 16HBE cells after 300 μM NNK stimulation for 48 h compared to other groups (Fig. 1E, F). Thus, we used 300 μM NNK to examine the time–response relationship of NNK-induced DNA damage.

As shown in Fig. 1G, a time-dependent increase in γ-H2AX levels was observed in NNK-treated 16HBE cells, with a more than fourfold elevation in γ-H2AX levels after 48-h exposure compared to control cells (Fig. 1G, H). Furthermore, immunofluorescence staining also revealed a time-dependent increase in γ-H2AX foci formation in NNK-treated cells after 2-h, 4-h, 8-h, 12-h, 24-h, and 48-h exposure (Fig. 1I). In particular, γ-H2AX foci formation was significantly increased after 48-h exposure to NNK compared to control cells (Fig. 1I, J). Similar NNK-induced DNA damage responses were observed in BEAS-2B cells (Figure S1). Our findings strongly suggest that NNK induces DNA damage in human bronchial epithelial cells.

NNK exposure causes inhibition of cell proliferation, and induction of cell cycle arrest and apoptosis in 16HBE cells

It is becoming increasingly clear that cumulative DNA damage can lead to cellular dysfunction, such as aberrant cell proliferation, cell cycle arrest and apoptosis, providing a link between DNA damage and disease progression (Evan and Vousden 2001; Jackson and Bartek 2009; Saitoh and Oda 2021). Therefore, we next examined the effects of NNK on cell proliferation in 16HBE cells using CCK8 and EdU assays. The CCK8 assay revealed that differences in cell proliferation between NNK-treated and control cells were observed after 48 h (Fig. 2A). Notably, NNK was found to have a growth-suppression effect on 16HBE cells relative to untreated cells. Similarly, the EdU assay revealed inhibition of cell proliferation in response to NNK treatment, with a significant reduction (approximately 50%) in cell proliferation rate after treatment with 300 μM NNK compared to the controls (Fig. 2B, C).

Since dysregulation of the cell cycle may be an underlying cause contributing to changes in cell proliferation (Aggarwal et al. 2020), we next examined the effects of NNK on the cell cycle in 16HBE cells. Flow cytometric analysis showed that the proportion of G2/M phase cells after NNK treatment was significantly increased in a dose-dependent manner, suggesting that NNK could lead to G2/M arrest in 16HBE cells (Fig. 2D, E). Notably, the most significant increase in G2/M cells was observed after exposure to 300 μM NNK compared to the negative control groups. Moreover, we found that NNK treatment induced a dose-dependent increase in the apoptosis rates of 16HBE cells (Fig. 2F, G). Taken together, our data suggest that NNK suppresses 16HBE cellular proliferation by blocking cell cycle progression and promoting the apoptosis of 16HBE cells.

Characterization of circNIPBL, which is up-regulated in NNK-treated human bronchial epithelial cells

To investigate the underlying mechanisms of NNK-induced DNA damage initiation, a PubMed literature search was carried out to identify miRNAs associated with DDR. A total of 40 miRNAs were identified as being relevant to DDR. Of them, 11 (hsa_miR-122-5p, hsa_miR-125b-5p,

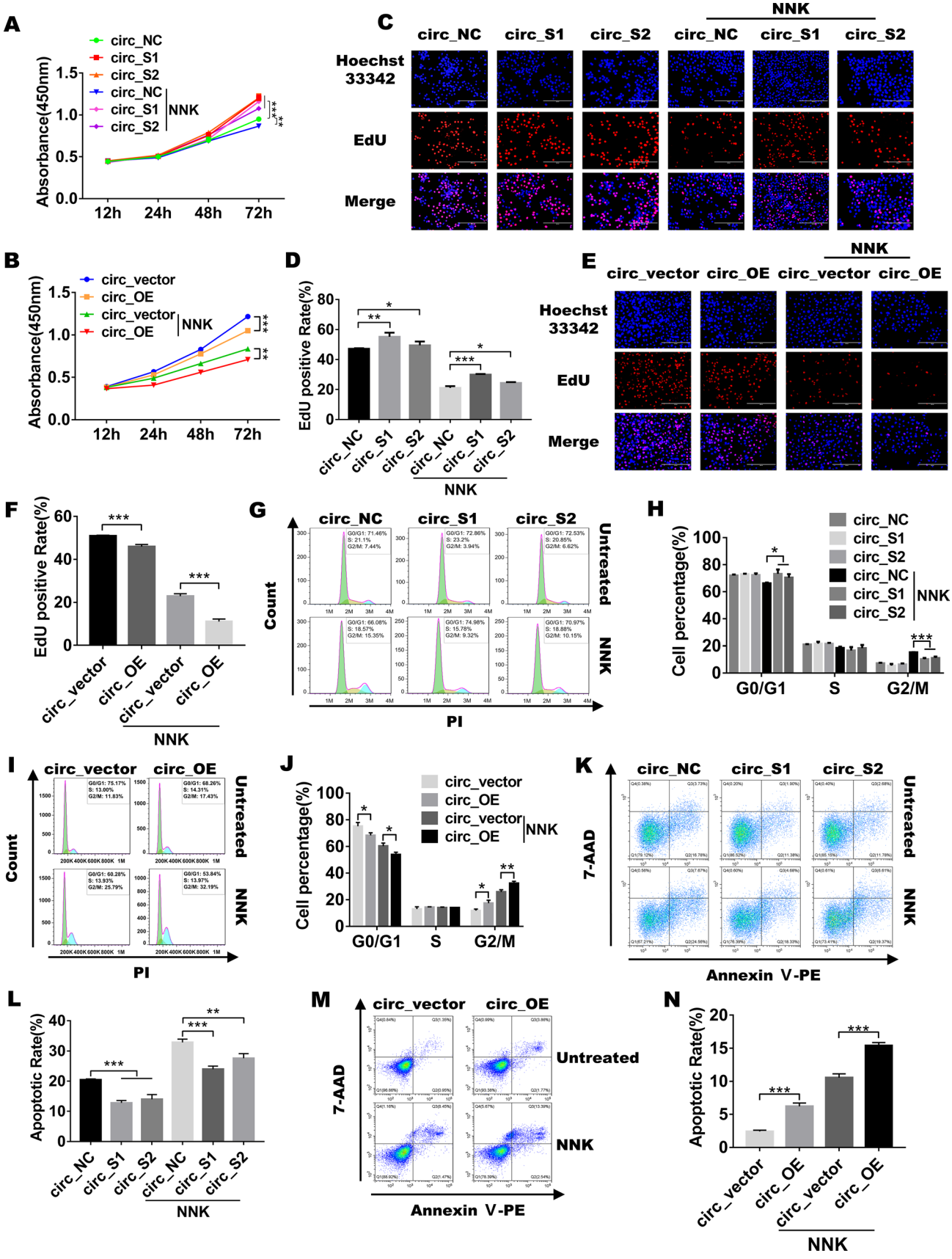
A
circ_NC
circ_S1
circ_S2
circ_NC
circ_S1
circ_S2
NNK
Absorbance(450nm)
12h
24h
48h
72h
B
circ_vector
circ_OE
circ_vector
circ_OE
NNK
C
NNK
circ_NC
circ_S1
circ_S2
circ_NC
circ_S1
circ_S2
Hoechst 33342
EdU
Merge
D
EdU positive Rate(%)
E
NNK
circ_vector
circ_OE
circ_vector
circ_OE
F
EdU positive Rate(%)
G
circ_NC
circ_S1
circ_S2
Untreated
NNK
Count
PI
H
circ_NC
circ_S1
circ_S2
circ_NC
circ_S1
circ_S2
NNK
Cell percentage(%)
G0/G1
S
G2/M
I
circ_vector
circ_OE
Untreated
NNK
Count
PI
J
circ_vector
circ_OE
circ_vector
circ_OE
NNK
Cell percentage(%)
G0/G1
S
G2/M
K
circ_NC
circ_S1
circ_S2
Untreated
NNK
7-AAD
Annexin V-PE
L
Apoptotic Rate(%)
M
circ_vector
circ_OE
Untreated
NNK
7-AAD
Annexin V-PE
N
Apoptotic Rate(%)
circ_vector
circ_OE
circ_vector
circ_OE
NNK

◂**Fig. 5** circNIPBL mediates NNK-induced anti-proliferation, cell cycle arrest and apoptosis in human bronchial epithelial cells. **A**, **B** Cell proliferation of circNIPBL-silenced or overexpressing 16HBE cells was assessed by CCK8 assays. **C–F** Proliferating cells were labeled using EdU after circNIPBL silencing or overexpression. **G–J** Flow cytometry analysis showing the cell cycle distribution of 16HBE cells. **K–N** Apoptosis rate of circNIPBL-silenced or overexpressing 16HBE cells was determined by flow cytometry

hsa_miR-126-5p, hsa_miR-145-5p, hsa_miR-146a-5p, hsa_miR-146b-5p, hsa_miR-181a-5p, hsa_miR-195-5p, hsa_miR-221-3p, hsa_miR-223-3p, and hsa_miR-24-3p) were used for further biological predictions since each miRNA was cited in more than 50 publications. Four circRNAs (hsa_circ_0001714, hsa_circ_0000990, hsa_circ_0001320, and hsa_circ_0001472) were found to bind to at least three of these miRNAs according to the StarBase database (http://starbase.sysu.edu.cn/), suggesting that they may have a potential role in the regulation of the DDR (Fig. 3A). We next detected the expression of four candidate circRNAs by qRT-PCR and found that circNIPBL (circBase ID: hsa_circ_0001472) was significantly up-regulated in 16HBE cells after treatment with 300 μM NNK for 48 h compared to controls (Fig. 3B). Further studies demonstrated that NNK exposure increased circNIPBL expression in a dose-dependent manner in 16HBE cells (Fig. 3C). Similar results were also observed in BEAS-2B cells based on qRT-PCR data (Fig. 3D). Thus, circNIPBL, derived from the NIPBL gene exon2-exon9 region, with a spliced length of 1574 bp, was selected as a candidate for further exploration in NNK-induced DNA damage (Fig. 3E).

Sanger sequencing for PCR products and RNase R treatment revealed that circNIPBL stably existed in a circular structure (Fig. 3E, F). In addition, nuclear and cytoplasmic fractionation assays demonstrated that circNIPBL expression was more abundant in the cytoplasm than the nucleus (Fig. 3G). Furthermore, FISH analysis revealed that circNIPBL was predominantly found in the cytoplasm (Fig. 3H). These findings suggest that circNIPBL is up-regulated in NNK-treated 16HBE cells and may have a potential biological role in the regulation of DNA damage.

CircNIPBL promotes NNK-induced DNA damage by mediating γ-H2AX levels

To determine whether circNIPBL was involved in the DNA damage caused by NNK exposure, we employed loss/gain of function approaches by silencing or overexpressing circNIPBL in 16HBE cells. As shown in Fig. 4A, B, circNIPBL expression was markedly decreased after transfected two siRNAs, and elevated approximately 12-fold after transfected by overexpression plasmid compared to the negative control group, while the linear RNA NIPBL transcript level was not significantly changed. The comet assay revealed that knockdown of circNIPBL significantly reduced NNK-induced DNA damage (Fig. 4C, D), while circNIPBL overexpression aggravated NNK-induced DNA damage (Fig. 4E, F). Next, we examined γ-H2AX protein expression levels after circNIPBL knockdown or overexpression by western blot analyses. We found that circNIPBL silencing significantly reduced γ-H2AX protein levels in NNK-treated and untreated 16HBE cells (Fig. 4G, H). Similarly, decreased γ-H2AX protein expression was observed in BEAS-2B cells transfected with circNIPBL siRNAs (Supplementary Figure S2A and B). In contrast, circNIPBL overexpression led to a significant increase in γ-H2AX expression in both 16HBE and BEAS-2B cells (Fig. 4I, J, Supplementary Figure S2C and D). DNA damage was also assessed by examining γ-H2AX foci formation in circNIPBL knockdown or overexpressing 16HBE cells. Compared to the negative controls, circNIPBL silencing caused a reduction in γ-H2AX foci in 16HBE cells (Fig. 4K, L). Consistent with the western blot data, a significant increase in γ-H2AX foci was also found in 16HBE cells after transfection with the circNIPBL overexpression plasmid (Fig. 4M, N). Taken together, our results strongly suggest that circNIPBL promotes NNK-induced DNA damage in human bronchial epithelial cells through the regulation of γ-H2AX expression.

circNIPBL mediates NNK-induced anti-proliferation, cell cycle arrest and apoptosis in human bronchial epithelial cells

To determine whether circNIPBL regulates NNK-induced anti-proliferation, cell cycle arrest and apoptosis, we examined the effects of circNIPBL knockdown and overexpression in 16HBE cells. As shown in Fig. 5A, circNIPBL knockdown resulted in a significant increase in cell proliferation in both untreated and NNK-treated 16HBE cells as measured by the CCK8 assay. In contrast, 16HBE cells exhibited a significant inhibition in proliferation after circNIPBL overexpression (Fig. 5B). Thus, our data suggest that circNIPBL enhances NNK-induced inhibition of 16HBE cell growth. We next confirmed the role of circNIPBL in mediating cell proliferation using an EdU assay. Our data demonstrated that in the presence of the negative siRNA (circ_NC) and overexpression vector (circ_OE) controls, NNK treatment decreased EdU staining by approximately 30% of EdU positive rates compared with control 16HBE cells, while NNK-induced inhibition of proliferation was reversed by circNIPBL knockdown and enhanced after circNIPBL overexpression (Fig. 5C–F). Having established

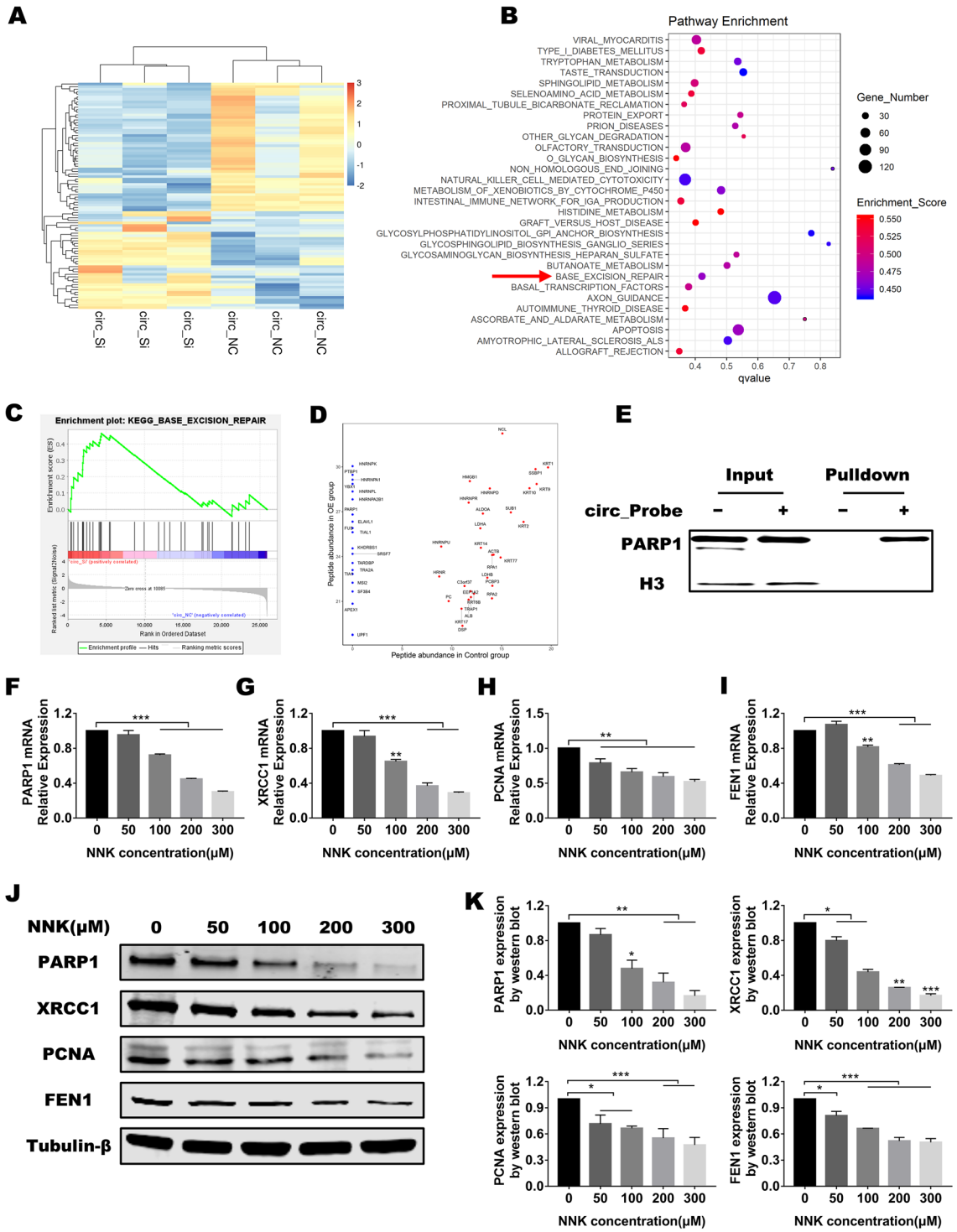

Fig. 6 The base excision repair pathway is involved in NNK-induced DNA damage regulation. **A** Differentially expressed mRNAs between circNIPBL-silenced and negative control-treated cells are shown as a heat map. **B** Bubble chart of the top 30 KEGG pathway enrichment scores by GSEA method. **C** Enrichment score diagram of the BER pathway. **D** Scatter plot of circNIPBL pull-down proteins. Blue plots indicate specific protein expression in circNIPBL pull-down elution, red plots indicate non-specific protein expression in both pull-down and input elutions. **E** Western blot analysis verifying the interaction between circNIPBL and PARP1. Histone H3 was used as a loading control. **F–I** qRT-PCR analysis showing PARP1, XRCC1, PCNA and FEN1 relative expression levels in NNK-treated 16HBE cells. **J**, **K** PARP1, XRCC1, PCNA and FEN1 protein expression levels were detected by western blot

that NNK treatment induced G2/M cell cycle arrest and subsequent inhibition of cell growth in 16HBE cells, we next sought to determine whether circNIPBL had a role in mediating cell cycle progression in NNK-treated cells. As shown in Fig. 5G, I, we found that silencing circNIPBL expression markedly increased G0/G1 cell cycle arrest in NNK-treated 16HBE cells, while the percentage of G2/M phase cells was significantly reduced as measured by flow cytometry. In contrast, circNIPBL overexpression led to a significant decrease in the percentage of G0/G1 phase cells, and substantial increase in G2/M-arrested cells in both untreated and NNK-treated 16HBE cells (Fig. 5H, J). The effects of circNIPBL on NNK-induced apoptosis were also examined by flow cytometry. We found that NNK treatment increased the rate of apoptosis in both two control groups (circ_NC and circ_vector). circNIPBL knockdown reversed NNK-induced apoptosis, while circNIPBL overexpression enhanced it (Fig. 5K–N). Together, these data demonstrate that up-regulation of circNIPBL inhibits cell proliferation by promoting cell cycle arrest in the G2/M phase and enhancing apoptosis in NNK-treated 16HBE cells.

The base excision repair pathway is involved in the regulation of NNK-induced DNA damage

To further understand the underlying mechanisms of circNIPBL in NNK-induced DNA damage, we performed mRNA sequencing (RNA-Seq) analysis to detect differential expression of mRNAs between circNIPBL-silenced and circ_NC-treated 16HBE cells. The differential mRNA expression profiles are shown in a cluster heat map (Fig. 6A). In total, 1274 mRNAs were identified as differentially expressed genes, of which 564 were significantly up-regulated and 710 were significantly down-regulated in circNIPBL-silenced 16HBE cells. Kyoto Encyclopedia of Genes and Genomes (KEGG) pathway enrichment analysis was evaluated by the Gene Set Enrichment Analysis (GSEA) method using the clusterProfiler package (https://doi.org/10.18129/B9.bioc.clusterProfiler). The top 30 related pathways are shown in a bubble chart in Fig. 6B. We identified the base excision repair (BER) pathway as a candidate pathway that showed promising correlation with circNIPBL, due to its high enrichment score and low false discovery rate when compared to other related pathways (Fig. 6B, C). Details of the enriched base excision repair genes are shown in Table S6. Next, mass spectrometry was used to validate the interactions between circNIPBL and DNA damage-associated proteins after a pull-down assay. We found that circNIPBL could interact with DNA repair proteins such as PARP1, FUS, and TIAL1 (Fig. 6D). However, only the interaction between circNIPBL and PARP1 protein was further confirmed by western blot analysis (Fig. 6E). In addition, we found that the expression levels of BER pathway genes such as PARP1, XRCC1, PCNA, and FEN1 were all significantly decreased after exposure to high concentrations of NNK (200 or 300 μM) as measured by qRT-PCR (Fig. 6F–I). PARP1, XRCC1, PCNA, and FEN1 protein expression levels were also reduced after NNK exposure, indicating that the BER pathway was involved in the regulation of NNK-induced DNA damage (Fig. 6J, K). Similarly, NNK treatment also inhibited expression of these BER proteins in BEAS-2B cells (Figure S3). Taken together, our results demonstrate that circNIPBL interacts with the PARP1 protein of the BER pathway, which participates in the modulation of NNK-induced DNA damage.

CircNIPBL promotes NNK-induced DNA damage via inhibition of the BER pathway

We next investigated the potential roles of circNIPBL in the regulation of the BER pathway in both 16HBE and BEAS-2B cells. We used siRNAs to knockdown the expression of circNIPBL, and found that PARP1, XRCC1, PCNA, and FEN1 protein levels were significantly increased in untreated 16HBE cells based on western blot analyses (Fig. 7A, B). Since our earlier data suggested that the inhibitory effect of NNK exposure on the BER pathway is through suppression of PARP1, XRCC1, PCNA, and FEN1 protein expression, we next examined whether circNIPBL silencing could rescue NNK-induced inhibition of the BER pathway. We found that circNIPBL silencing successfully increased PARP1, XRCC1, PCNA, and FEN1 protein expression in NNK-induced16HBE cells (Fig. 7A, B). Similar results demonstrating that circNIPBL knockdown could reverse the NNK-induced inhibition of the BER pathway were also observed in BEAS-2B cells (Fig. 7C, D). Subsequently, we overexpressed circNIPBL in 16HBE cells with or without NNK treatment. We found that overexpression of circNIPBL dramatically decreased PARP1, XRCC1, PCNA, and FEN1 protein expression compared to negative controls in 16HBE cells (Fig. 7E, F). Of note, circNIPBL overexpression combined with NNK treatment exhibited the most significant reduction in PARP1, XRCC1, PCNA, and FEN1 protein levels in 16HBE cells, suggesting that circNIPBL has an important role in the regulation of NNK-induced DNA damage. In addition, we further verified that circNIPBL overexpression also decreased the expression of BER pathway-associated proteins in BEAS-2B cells (Fig. 7G, H). Collectively, our data demonstrate that circNIPBL plays a critical role

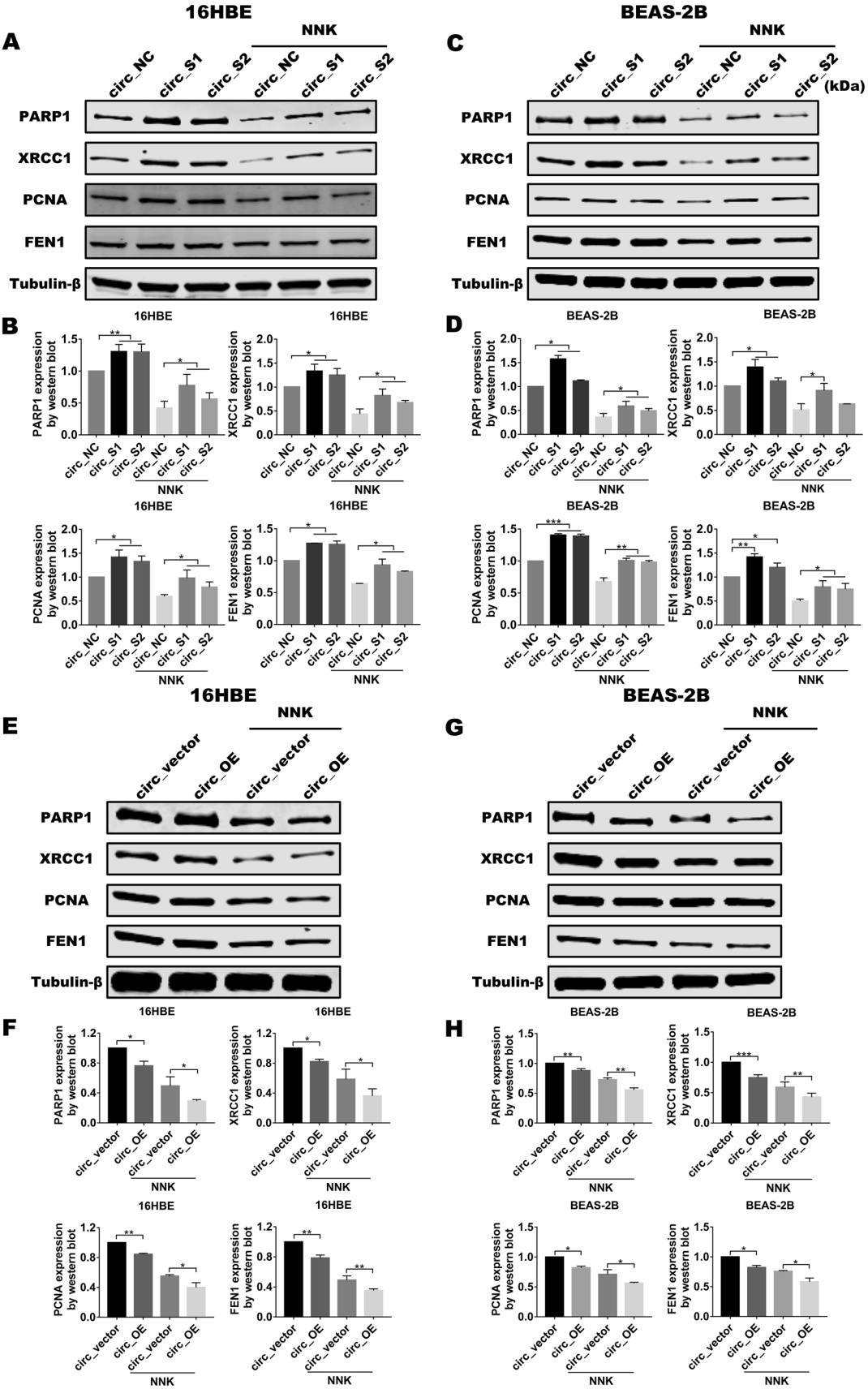
16HBE
BEAS-2B
A
C
NNK
circ_NC
circ_S1
circ_S2
circ_vector
circ_OE
PARP1
XRCC1
PCNA
FEN1
Tubulin-β
(kDa)
B
D
E
G
F
H
PARP1 expression by western blot
XRCC1 expression by western blot
PCNA expression by western blot
FEN1 expression by western blot

◂**Fig. 7** CircNIPBL promotes NNK-induced DNA damage via inhibition of the BER pathway. **A**, **B** Western blot analysis and quantification of BER-associated protein expression in circNIPBL-silenced-16HBE cells. **C**, **D** Western blot analysis and quantification of BER-associated protein expression in circNIPBL-silenced BEAS-2B cells. **E**, **F** Western blot analysis and quantification of BER-associated protein expression in circNIPBL-overexpressing 16HBE cells. **G**, **H** Western blot analysis and quantification of BER-associated protein expression in circNIPBL-overexpressing BEAS-2B cells. Protein bands were normalized to tubulin-β

in modulating the BER pathway and thus regulates NNK-induced DNA damage.

Discussion

DNA damage is generally considered to be the initiating process of carcinogenesis, and damaged DNA that is not properly repaired may lead to genomic instability, apoptosis, or senescence, which in turn are implicated in cancer development (Guo et al. 2019; Saitoh and Oda 2021; Schiewer and Knudsen 2019). It is well established that nuclear DNA is the target for various genotoxic agents present in cigarette smoke, and thus may result in DNA damage, such as double-strand breaks in human bronchial epithelial cells (Amararathna et al. 2020; Zhao et al. 2009). NNK, a type of tobacco-specific nitrosamine, has been confirmed to be a carcinogen in lung tumorigenesis in our previous in vivo studies (Wu et al. 2013). In the present study, we further investigated the potential role of NNK in cellular DNA damage, and examined its underlying mechanisms to provide clues for revealing the etiology of NNK-induced carcinogenesis. We demonstrated that NNK exposure induced DNA damage in 16HBE and BEAS-2B cells, and identified a circRNA, circNIPBL, that was up-regulated in NNK-treated 16HBE and BEAS-2B cells, and was correlated with NNK-induced DNA damage. Moreover, circNIPBL was found to promote NNK-induced DNA damage through modulation of the BER pathway and interactions with the DNA repair protein, PARP1. To the best of our knowledge, this is the first report to describe the potential role of circRNAs in the regulation of DNA damage caused by environmental chemicals.

In response to DNA lesions induced by various environmental genotoxic agents, normal cells can initiate a specific cellular response, defined as DNA damage response (DDR), to maintain genome integrity (Arjumand et al. 2018; Dietlein and Reinhardt 2014; Zhang and Peng 2015). The function of the DDR is to permit normal cells to repair DNA damage or if the lesions are beyond repair, arrest cell cycle progression and activate the apoptosis pathway (Arjumand et al. 2018; Dietlein and Reinhardt 2014). In this study, we found that NNK exposure caused DSBs in both 16HBE and BEAS-2B cells with increased γ-H2AX protein expression and γ-H2AX foci formation. γ-H2AX is considered to be a marker for DSBs. DSBs are a huge threat and result in genome instability, mutations, cell death, and tumorigenesis if they cannot be correctly repaired (Barnes et al. 2018; George and Rupasinghe 2017; Ibuki et al. 2015). Here, we observed apoptosis and cell cycle arrest in 16HBE cells after NNK treatment, which ultimately led to cell growth suppression and elimination of cells with excessive DNA damage. Multiple studies have demonstrated that noncoding RNAs (ncRNAs), such as miRNAs and lncRNAs, are emerging as critical players in DNA damage repair and have an essential role in maintaining cell survival and normal function (Arjumand et al. 2018). For example, Lai et al. showed that miR-7-5p impeded DSB repair caused by doxorubicin through reducing the expression of BRCA1 and Rad51, two sensitive markers for homologous recombination repair (Lai et al. 2019). LncRNA SNHG12 was identified as an important regulator of genomic stability because of its crucial role in interacting with DNA-dependent protein kinase (DNA-PK), a key mediator of the DDR, in atherosclerotic lesions (Haemmig et al. 2020). Recently, the emergence of circRNAs has provided a better understanding of the mechanisms of numerous cellular processes, and further provided new insights into the regulation of DNA damage. To date, several circRNAs such as circITCH, CDR1as, and cCNTNAP3, have been found to be associated with the modulation of DNA damage (Han et al. 2020; Lou et al. 2020; Wang et al. 2020a). Importantly, our study was the first to elucidate the mechanism of circRNA in chemical carcinogen-induced DNA damage. We found that knockdown of circNIPBL decreased γ-H2AX protein levels and repressed γ-H2AX foci formation, while overexpression of circNIPBL had the opposite effect, suggesting that circNIPBL accelerates NNK-induced DNA damage.

Mechanistically, we found that circNIPBL silencing significantly elevated PARP1, XRCC1, PCNA, and FEN1 protein levels, whereas overexpression of circNIPBL caused a significant decrease in BER pathway activity. Poly (ADP-ribose) polymerase 1 (PARP1), functions as a key enzyme in the BER pathway, and has been reported to play important roles in numerous biological processes, such as DNA repair, chromatin remodeling, and transcription (Thomas and Tulin 2013). Here, we found that PARP1 protein levels were significantly repressed by NNK treatment in a dose-dependent manner, indicating an essential role in response to DSB repair. A direct interaction between PARP1 and histone H2AX has been previously described in mammalian cells after exposure to ionizing

irradiation, which induces DSBs, and promotes rapid phosphorylation of H2AX (Du et al. 2006; Thomas and Tulin 2013). Similarly, our data confirmed that simultaneous changes in PARP1 and γ-H2AX levels occurred after NNK treatment, strongly suggesting that both proteins have an important role in the regulation of NNK-induced DNA damage. As previously reported, the recruitment of XRCC1 by PARP1 after DNA damage was considered to be a key step for the recruitment of downstream repair enzymes (Nassour et al. 2016). Interestingly, we found that PARP1, XRCC1, PCNA, and FEN1 protein expression was significantly suppressed by NNK, while circNIPBL was shown to interact with PARP1 protein. Furthermore, we demonstrated that overexpression of circNIPBL could dramatically exacerbate NNK-induced DNA damage and cell apoptosis through interacting with PARP1 and decreasing its protein expression. However, the potential mechanisms by which circNIPBL regulates reduced PARP1 expression, such as promoting its ubiquitination, were not examined here, and will be the focus of future studies.

Conclusions

In summary, our study demonstrated the promotive effects of circNIPBL in NNK-induced DNA damage and cellular dysfunction. Further mechanistic analysis revealed that circNIPBL promotes NNK-induced DNA damage by suppressing the BER pathway and interacting with the DNA repair protein, PARP1. Taken together, our findings provide new evidence that circRNAs have a critical role in mediating environmental carcinogen-induced cellular DNA damage, as well as provide novel insights into understanding environmental carcinogenesis.

Supplementary Information The online version contains supplementary material available at https://doi.org/10.1007/s00204-022-03297-z.

Author contributions YL: conceptualization, methodology, data curation, validation, visualization, writing—original draft. QH: conceptualization, investigation, writing—original draft. ML: validation, methodology. XL: validation, methodology. WC: methodology. HZ: methodology. QD: methodology. CS: software, formal analysis. YL: investigation. YJ: resources, supervision, writing—review and editing, project administration, funding acquisition.

Funding This study was supported by the National Natural Science Foundation of China (82130095, 91643204, 81872652 to J.Y.), Guangdong Natural Science Foundation (2018B030311019 to J.Y.), Open Research Fund of the Sixth Affiliated Hospital of Guangzhou Medical University, Qingyuan People's Hospital (202011-108 to J.Y.), and the Key Medical Disciplines and Specialties Program of Guangzhou (2021-2023).

Declarations

Conflict of interest The authors declare that they have no known competing financial interests or personal relationships that could have appeared to influence the work reported in this paper.

References

Aggarwal V, Tuli HS, Tania M et al (2020) Molecular mechanisms of action of epigallocatechin gallate in cancer: recent trends and advancement. Semin Cancer Biol. https://doi.org/10.1016/j.semcancer.2020.05.011

Amararathna M, Hoskin DW, Rupasinghe HPV (2020) Anthocyanin-rich haskap (*Lonicera caerulea* L.) berry extracts reduce nitrosamine-induced DNA damage in human normal lung epithelial cells in vitro. Food Chem Toxicol 141:111404. https://doi.org/10.1016/j.fct.2020.111404

Arjumand W, Asiaf A, Ahmad ST (2018) Noncoding RNAs in DNA damage response: opportunities for cancer therapeutics. Methods Mol Biol 1699:3–21. https://doi.org/10.1007/978-1-4939-7435-1_1

Balbo S, Johnson CS, Kovi RC et al (2014) Carcinogenicity and DNA adduct formation of 4-(methylnitrosamino)-1-(3-pyridyl)-1-butanone and enantiomers of its metabolite 4-(methylnitrosamino)-1-(3-pyridyl)-1-butanol in F-344 rats. Carcinogenesis 35(12):2798–2806. https://doi.org/10.1093/carcin/bgu204

Barnes JL, Zubair M, John K, Poirier MC, Martin FL (2018) Carcinogens and DNA damage. Biochem Soc Trans 46(5):1213–1224. https://doi.org/10.1042/BST20180519

Basu AK (2018) DNA damage, mutagenesis and cancer. Int J Mol Sci. https://doi.org/10.3390/ijms19040970

Brown PJ, Massey TE (2009) In vivo treatment with 4-(methylnitrosamino)-1-(3-pyridyl)-1-butanone (NNK) induces organ-specific alterations in in vitro repair of DNA pyridyloxobutylation. Mutat Res 663(1–2):15–21. https://doi.org/10.1016/j.mrfmmm.2008.12.008

Dietlein F, Reinhardt HC (2014) Molecular pathways: exploiting tumor-specific molecular defects in DNA repair pathways for precision cancer therapy. Clin Cancer Res 20(23):5882–5887. https://doi.org/10.1158/1078-0432.CCR-14-1165

Doukas SG, Vageli DP, Lazopoulos G, Spandidos DA, Sasaki CT, Tsatsakis A (2020) The effect of NNK, A tobacco smoke carcinogen, on the miRNA and mismatch DNA repair expression profiles in lung and head and neck squamous cancer cells. Cells. https://doi.org/10.3390/cells9041031

Du YC, Gu S, Zhou J et al (2006) The dynamic alterations of H2AX complex during DNA repair detected by a proteomic approach reveal the critical roles of Ca(2+)/calmodulin in the ionizing radiation-induced cell cycle arrest. Mol Cell Proteom 5(6):1033–1044. https://doi.org/10.1074/mcp.M500327-MCP200

Evan GI, Vousden KH (2001) Proliferation, cell cycle and apoptosis in cancer. Nature 411(6835):342–348. https://doi.org/10.1038/35077213

George VC, Rupasinghe HPV (2017) Apple flavonoids suppress carcinogen-induced DNA damage in normal human bronchial epithelial cells. Oxid Med Cell Longev 2017:1767198. https://doi.org/10.1155/2017/1767198

Guo H, Liu H, Wu H et al (2019) Nickel carcinogenesis mechanism: DNA damage. Int J Mol Sci. https://doi.org/10.3390/ijms20194690

Haemmig S, Yang D, Sun X et al (2020) Long noncoding RNA SNHG12 integrates a DNA-PK-mediated DNA damage response and vascular senescence. Sci Transl Med 12:531

Han D, Wang Y, Wang Y et al (2020) The tumor-suppressive human circular RNA CircITCH sponges miR-330-5p to ameliorate doxorubicin-induced cardiotoxicity through upregulating SIRT6, survivin, and SERCA2a. Circ Res 127(4):e108–e125. https://doi.org/10.1161/CIRCRESAHA.119.316061

Hua Q, Chen Y, Liu Y et al (2019) Circular RNA 0039411 is involved in neodymium oxide-induced inflammation and antiproliferation in a human bronchial epithelial cell line via sponging miR-93-5p. Toxicol Sci 170(1):69–81. https://doi.org/10.1093/toxsci/kfz074

Hua Q, Liu Y, Li M et al (2021) Tobacco-related exposure upregulates Circ_0035266 to exacerbate inflammatory responses in human bronchial epithelial cells. Toxicol Sci 179(1):70–83. https://doi.org/10.1093/toxsci/kfaa163

Ibuki Y, Shikata M, Toyooka T (2015) gamma-H2AX is a sensitive marker of DNA damage induced by metabolically activated 4-(methylnitrosamino)-1-(3-pyridyl)-1-butanone. Toxicol in Vitro 29(7):1831–1838. https://doi.org/10.1016/j.tiv.2015.07.023

Jackson SP, Bartek J (2009) The DNA-damage response in human biology and disease. Nature 461(7267):1071–1078. https://doi.org/10.1038/nature08467

Jia Y, Li X, Nan A et al (2020) Circular RNA 406961 interacts with ILF2 to regulate PM(2.5)-induced inflammatory responses in human bronchial epithelial cells via activation of STAT3/JNK pathways. Environ Int 141:105755. https://doi.org/10.1016/j.envint.2020.105755

Konstantinou E, Fotopoulou F, Drosos A et al (2018) Tobacco-specific nitrosamines: a literature review. Food Chem Toxicol 118:198–203. https://doi.org/10.1016/j.fct.2018.05.008

La Maestra S, Kisby GE, Micale RT et al (2011) Cigarette smoke induces DNA damage and alters base-excision repair and tau levels in the brain of neonatal mice. Toxicol Sci 123(2):471–479. https://doi.org/10.1093/toxsci/kfr187

Lai J, Yang H, Zhu Y, Ruan M, Huang Y, Zhang Q (2019) MiR-7-5p-mediated downregulation of PARP1 impacts DNA homologous recombination repair and resistance to doxorubicin in small cell lung cancer. BMC Cancer 19(1):602. https://doi.org/10.1186/s12885-019-5798-7

Levine AJ, Oren M (2009) The first 30 years of p53: growing ever more complex. Nat Rev Cancer 9(10):749–758. https://doi.org/10.1038/nrc2723

Li X, Wu J, Zheng J et al (2013) Altered miRNA expression profiles and miR-1a associated with urethane-induced pulmonary carcinogenesis. Toxicol Sci 135(1):63–71. https://doi.org/10.1093/toxsci/kft131

Li X, Yang L, Chen LL (2018) The biogenesis, functions, and challenges of circular RNAs. Mol Cell 71(3):428–442. https://doi.org/10.1016/j.molcel.2018.06.034

Lou J, Hao Y, Lin K et al (2020) Circular RNA CDR1as disrupts the p53/MDM2 complex to inhibit gliomagenesis. Mol Cancer 19(1):138. https://doi.org/10.1186/s12943-020-01253-y

Luo K, Qin Y, Ouyang T et al (2021) let-7c-5p regulates CyclinD1 in fluoride-mediated osteoblast proliferation and activation. Toxicol Sci. https://doi.org/10.1093/toxsci/kfab054

Malakoti F, Alemi F, Younesi S et al (2021) The cross-talk between signaling pathways, noncoding RNAs and DNA damage response: emerging players in cancer progression. DNA Repair (Amst) 98:103036. https://doi.org/10.1016/j.dnarep.2020.103036

Nassour J, Martien S, Martin N et al (2016) Defective DNA single-strand break repair is responsible for senescence and neoplastic escape of epithelial cells. Nat Commun 7:10399. https://doi.org/10.1038/ncomms10399

Pan X, Yuan X, Li X et al (2019) Induction of inflammatory responses in human bronchial epithelial cells by Pb(2+)-containing model PM(2.5) particles via downregulation of a novel long noncoding RNA lnc-PCK1-2:1. Environ Sci Technol 53(8):4566–4578. https://doi.org/10.1021/acs.est.8b06916

Poirier MC (2004) Chemical-induced DNA damage and human cancer risk. Nat Rev Cancer 4(8):630–637. https://doi.org/10.1038/nrc1410

Roos WP, Thomas AD, Kaina B (2016) DNA damage and the balance between survival and death in cancer biology. Nat Rev Cancer 16(1):20–33. https://doi.org/10.1038/nrc.2015.2

Saitoh T, Oda T (2021) DNA damage response in multiple myeloma: the role of the tumor microenvironment. Cancers (basel). https://doi.org/10.3390/cancers13030504

Schiewer MJ, Knudsen KE (2019) DNA damage response in prostate cancer. Cold Spring Harb Perspect Med. https://doi.org/10.1101/cshperspect.a030486

Thomas C, Tulin AV (2013) Poly-ADP-ribose polymerase: machinery for nuclear processes. Mol Asp Med 34(6):1124–1137. https://doi.org/10.1016/j.mam.2013.04.001

Wang H, Song X, Wang Y et al (2020a) CircCNTNAP3-TP53-positive feedback loop suppresses malignant progression of esophageal squamous cell carcinoma. Cell Death Dis 11(11):1010. https://doi.org/10.1038/s41419-020-03217-y

Wang X, Li H, Lu Y, Cheng L (2020b) Circular RNAs in human cancer. Front Oncol 10:577118. https://doi.org/10.3389/fonc.2020.577118

Wu J, Yang T, Li X et al (2013) Alteration of serum miR-206 and miR-133b is associated with lung carcinogenesis induced by 4-(methylnitrosamino)-1-(3-pyridyl)-1-butanone. Toxicol Appl Pharmacol 267(3):238–246. https://doi.org/10.1016/j.taap.2013.01.002

Xiao Z, Yang Z, Xu M et al (2021) The Circ_CARM1 controls cell migration by regulating CTNNBIP1 in anti-benzo[a]pyrene-trans-7,8-dihydrodiol-9,10-epoxide-transformed 16HBE cells. Toxicol Lett 348:40–49. https://doi.org/10.1016/j.toxlet.2021.05.007

Yoshida K, Gowers KHC, Lee-Six H et al (2020) Tobacco smoking and somatic mutations in human bronchial epithelium. Nature 578(7794):266–272. https://doi.org/10.1038/s41586-020-1961-1

Zhang C, Peng G (2015) Non-coding RNAs: an emerging player in DNA damage response. Mutat Res Rev Mutat Res 763:202–211. https://doi.org/10.1016/j.mrrev.2014.11.003

Zhao H, Albino AP, Jorgensen E, Traganos F, Darzynkiewicz Z (2009) DNA damage response induced by tobacco smoke in normal human bronchial epithelial and A549 pulmonary adenocarcinoma cells assessed by laser scanning cytometry. Cytometry A 75(10):840–847. https://doi.org/10.1002/cyto.a.20778